Air-clad photonic lanterns: fabrication and applications

Mathew, Neethu Mariam; Grüner-Nielsen, Lars; Lillieholm, Mads; Galili, Michael; Rottwitt, Karsten

Published in:
Journal of Optics

Link to article, DOI:
10.1088/2040-8986/ac5f23

Publication date:
2022

Document Version
Peer reviewed version

Journal of Optics

ACCEPTED MANUSCRIPT

Air-clad photonic lanterns: fabrication and applications

To cite this article before publication: Neethu Mariam Mathew *et al* 2022 *J. Opt.* in press https://doi.org/10.1088/2040-8986/ac5f23

Air-clad photonic lanterns: Fabrication and applications.

Neethu Mariam Mathew [1], Lars Grüner-Nielsen [1,2], Mads Lillieholm [1], Michael Galili [1], Karsten Rottwitt [1]

[1] DTU Fotonik, Ørsteds Plads, building 343, 2800 Kgs. Lyngby, Denmark,
[2] Danish Optical Fiber Innovation, Åvendingen 22A, 2700 Brønshøj, Denmark

E-mail: namama@fotonik.dtu.dk

October 2021

Abstract. The fabrication steps for an air-clad photonic lantern that can excite the first two LP mode groups in a multimode fiber are presented in this paper. A multiplexing crosstalk below -16.8 dB is measured on the fabricated lantern using S^2 imaging technique over a wavelength of 1525 nm to 1575 nm. The de-multiplexing crosstalk is measured for both LP_{01} and LP_{11} mode groups as -16.8 dB and -9.4 dB respectively using loss measurements. 2×40 Gb/s MIMO-less MDM transmission through 7 m of two mode step index fiber is demonstrated using the fabricated photonic lanterns. 2×10 Gb/s MIMO-less MDM transmission through 1.6 km standard 50/125 µm multimode fiber is also demonstrated and a Q value higher than 3.7 is obtained for both spatial channels over all input polarizations. Simple intensity modulation and direct detection schemes are used for these MDM transmissions.

1. Introduction

Ever since, Charles Kao's invention of optical fiber [1, 2], there is a constant search of ways to improve the optical data transmission capacity through optical communication networks. The development of Erbium doped amplifier (EDFA) and wavelength division multiplexing (WDM) networks has contributed a great deal to this improvement. Advanced modulation techniques like Quadrature amplitude modulation (QAM), and coherent detection using intradyne receivers could further push the data capacity limits to the Tb/s level. In spite of all these advancements, the capacity growth in communication systems is showing signs of saturation, while the required data traffic is continuing its strong growth [3]. Scaling of the data transport system in the space dimension is a possible solution to the imminent capacity crunch problem. This kind of parallel transmission through different spatial channels is in general termed as space division multiplexing (SDM). Mode divison multiplexing (MDM) is one type of SDM approach, where multiple spatial modes in a single large core fiber are used for parallel transmission of data. Larger the core size, or larger the refractive index difference

between the core and the cladding, the more number of spatial modes can be supported by the multimode fiber.

Fiber modes are solutions to the eigen value equation, derived from the Maxwell equations for a circularly symmetric fiber crosssection. Solving the eigen equation gives the propagation constant of the mode β as the eigen value and the electic field distribution as the eigen vector. The effective index value n_{eff} of the modes can be obtained from propagation constant β as

$$n_{eff} = \frac{\beta}{k_0} \tag{1}$$

where k_0 is the vacuum wavenumber. n_{eff} is the refractive index that light sees within the waveguide and will have a value between the core index and cladding index of the fiber.

For optical fibers, the refractive index difference between the core and cladding is very small, and hence it is reasonable to approximate the derivative of the dielectric function ϵ in the eigen value equation to 0. This approximation is termed as the weakly guided approximation or the scalar approximation [4]. Solutions of scalar equation are called linearly polarized, LP modes and are denoted as LP_{ml}, where $2m$ is the number of zero crossings on the field distribution when going around a full circle at a constant radius and $l-1$ is the number of zero crossings when going out into the radial direction. Vector mode solutions obtained without any scalar approximation are the true Eigen modes of the fiber, but due to slight index changes in the fiber from fabrication uncertainties, there will be mixing of vector modes. Hence a normal multi mode fiber only supports the stable propagation of LP mode groups. A two mode fiber is a few mode fiber (FMF) that can support the LP_{01} and LP_{11} mode groups [5]. The LP_{11} mode group include the LP_{11a} and LP_{11b} degenerate modes with the same propagation constant.

Building MDM transmission systems with multimode fibers has some component and connectivity challenges. One is the efficient excitation and splitting of higher order modes from the fundamental LP_{01} mode. A spatial multiplexer (MUX) and de-multiplexer (DMUX) allows to combine and separate the spatial channels in and out of a FMF. With mode selective MUX and DMUX, it is possible to selectively multiplex and de-multiplex a specific mode into and out of the FMF.

Different techniques for mode multiplexing and de-multiplexing has been developed and tested in transmission systems in the past decade. A large part of these include free space setups like binary phase plates, spatial light modulator(SLM) [6] and multi-plane light conversion techniques [7]. These free space mode convertors need extra components to couple the generated mode into the fiber, which generally introduce extra insertion losses and spatial crosstalks between the channels. Compact fiber based mode convertors would be a better solution, as they can be spliced directly to a transmission fiber. A mode selective photonic lantern is such a fiber based device that works by the principle of tapered mode transition. Unlike other fiber based mode convertors like long period gratings (LPG) [8,9], and fused biconic couplers [10], which are resonant devices, based

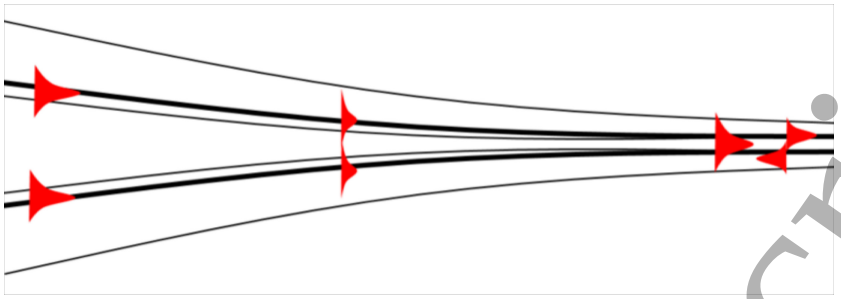

Figure 1. Transition of SMF modes to higher order modes in a photonic lantern.

on a phase matching condition at a narrow wavelength band, photonic lanterns are wide bandwidth devices, which makes them compatible with WDM systems.

2. Photonic Lanterns

A photonic lantern (PL) is a fiber based mode convertor that can efficiently transform light from different single mode fibers to light in multimodes and vice versa. In the conventional fabrication method, different SMFs are stranded together and inserted in a Fluorine doped low refractive index capillary tube and the SM fiber bundle is tapered down together with the outer capillary tube [11]. As the SM fiber is tapered down to smaller diameter, the SMF cores start coupling light out of their individual cores and the LP_{01} modes gradually transforms into multimode fiber modes at the end of the taper as shown in the sketch in fig 1. At the end of the fiber bundle taper, the original SMF cores will be very thin and hence insignificant, while the silica cladding of the fibers together form the new core and the outer low index capillary tube form the new cladding. Thus a multimode waveguide that can support higher order modes is formed at the taper end. When the SMFs used in the fabrication are all identical, the PL is termed as non mode selective. In a non mode selective PL, there will be mixing of modes, and light launched at either of the SMFs can excite a combination of all the available modes supported by the multimode waveguide at the taper end. Non mode selective photonic lanterns were initially used in some MDM transmissions, but highly computational multiple input multiple output digital signal processing (MIMO-DSP) is required to separate the spatial channels from their linear combination states. Coherent MIMO transmission in a FMF that can support six spatial channels and 32 WDM channels, through a distance of 900 km is reported using non mode selective PLs. [12]. A mode selective PL can reduce the complexity of MIMO processing, as it can excite a specific LP mode in a FMF using a specific SM input fiber. To introduce mode selectivity in a photonic lantern, we have to break the degeneracy of the SMF modes, by using dissimilar SMFs. The dissimilarity can be either in the core size or refractive index of the SMFs. Within a FMF, there will be mixing between the degenerate LP modes, for example, between LP_{11a} and LP_{11b} modes. Hence a PL that can excite a specific mode group in a FMF is enough. Relatively simple MIMO can be used to separate the

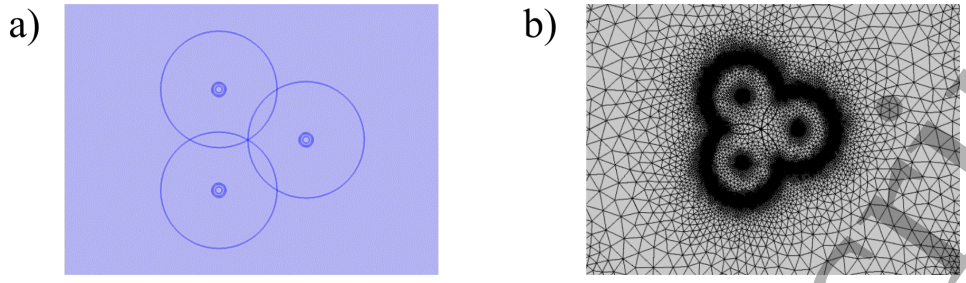

Figure 2. a) Geometrical arrangement of three identical fibers of a non mode selective lantern. b) The physics controlled mesh used for the mode analysis.

degenerate channels within a mode group or MIMO can be fully avoided if the entire mode group is used as a single channel. A PL that can excite the first two mode groups namely LP_{01} and LP_{11} can be fabricated using three SMFs, where one fiber should be dissimilar from the other two. Similary to exite the first four mode groups namely LP_{01}, LP_{11}, LP_{21} and LP_{02}, six SMFs are required, which includes four dissimilar types of SMFs. PLs that could excite up to six LP modes, having an insertion loss of 1.9 dB and crosstalk of -9 dB has been reported [13].

3. Air-clad photonic lanterns

The low refractive index capillary tubes used for PL fabrication is not that easily accessible. The number of SMFs used for the fabrication scales up with the number of modes needed. Uniform tapering of capillary tubes of larger diameter in a glass processor using heating filament is difficult. Hence a more simple and cost effective fabrication technique is tried, where the outer capillary tube is not used [14, 15]. The air surrounding the taper form the low index cladding, that guides the light through the taper, hence they are termed air-clad PLs. Air clad PLs that could excite the first two LP mode groups are fabricated using two kinds of three SMFs and the fabricated devices are tested on MDM transmission setups. These results on the design, fabrication and characterization of air-clad PLs and their application in MDM transmission are described in this paper.

4. Design

The mode evolution along the taper is studied by solving the eigen equation at different 2D cross sections of the taper. This is done with a a full vectorial mode solver using the wave optics module in COMSOL Multiphysics and also a scalar mode solver written in Python, where scalar approximation is used. A non mode selective PL with three identical True Wave fibers is modelled first. The three fibers are centered along the vertices of an equilateral triangle as shown in the fig 2a. COMSOL uses the finite element method to solve the frequency domain form of Maxwell equation. A finer physics controlled mesh is used for the mode analysis as shown in the fig 2b. 2D cross sections

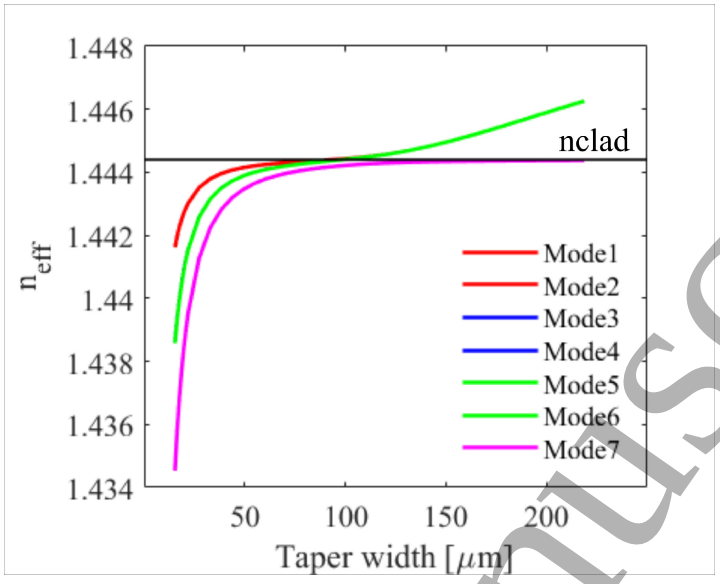

Figure 3. The variation of effective index for the first seven vector modes with taper width for a non mode selective PL.

at different points along the taper is obtained by scaling down the three cladding and core diameters by multiplying with a factor. At each 2D plane, the refractive indices of the core and cladding of the fibers and the outer air cladding are included in the calculation. The calculated effective index values of the first seven vector modes are plotted as a function of taper width in fig 3. Before tapering, the three fiber bundle has a width around 219 μm. In the beginning of the taper, light is well confined in the three SMF cores giving six degenerate fundamental modes with the same effective index values. The seventh mode is a cladding mode with a n_{eff} smaller than the silica cladding (nclad). As the taper width decreases, the n_{eff} of the first six modes separates into two groups. The degeneracy of the six modes in the beginning of the taper results in the mixing of light in a non mode selective PL.

Mode evolution in a mode selective taper is studied next using the 2D mode solver in COMSOL. To introduce mode selectivity between the LP_{01} and LP_{11} mode groups, a dissimilarity is introduced in one of the three fibers. This dissimilarity will break the degeneracy of the fundamental modes in the beginning of the taper, as their propagation constants are different. The light in the input fiber that supports the mode with the highest propagation constant, will evolve into a taper mode with the highest effective index and the rest accordingly. The fibers selected for the mode selective PL are a Thorlabs SM 2000 fiber and and two OFS ClearLite 16 fibers. The fibers differ both in core diameter and core index as shown in table 1. The silica cladding diameter and refractive index are 125 μm and 1.4444 respectively. The same geometrical arrangement as in fig 2a is used for the mode analysis. The SM2000 fiber with larger core is placed on the right and the two OFS ClearLite 16 fibers on the left side of the structure. The core and cladding indices of the three fibers and the outer air cladding are set according to their respective values and the mode solutions are calculated at different taper widths

Name	Core diameter [µm]	core index @1550
SM2000	11	1.4499
OFS CL	4	1.4530

Table 1. The core diameter and refractive index of SM 2000 and OFS CL fibers used for the fabrication of mode selective lantern.

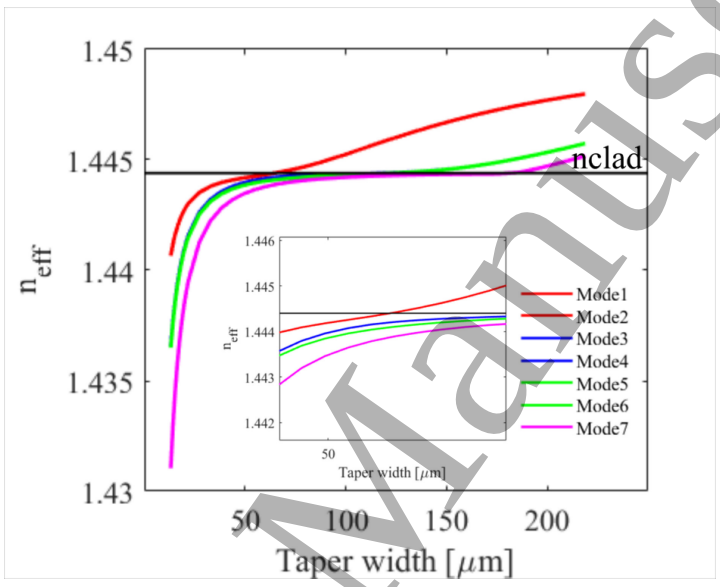

Figure 4. The variation of effective index for the first seven vector modes with taper width for a mode selective PL.

by scaling down the whole geometry. The solution gives the set of n_{eff} values and field distributions of the modes supported by the waveguide at different 2D cross sections of the taper. The calculated n_{eff} values as a function of taper width for this mode selective taper is shown in fig 4. The electric field distributions of the first six taper modes at a taper width of 19 µm is shown in fig 5. The magnitude of the complex field $\sqrt{E_x^2 + E_y^2 + E_z^2}$ is plotted here. Mode 1 and mode 2 form the LP_{01} mode group and mode 3 to mode 6 form the LP_{11} mode group. The n_{eff} of the fundamental mode in SM2000 fiber is larger than the n_{eff} for the fundamental mode of OFS CL fibers. Hence light launched into the SM2000 fiber will evolve into a taper mode with the highest n_{eff} and it could be called the LP_{01} like taper mode as this mode can excite the real LP_{01} mode in a FMF. While light launched into either of the OFS CL fibers will evolve into an LP_{11} like taper mode which can excite a combination of LP_{11a} and LP_{11b} mode in the FMF. Eventough the n_{eff} values of LP_{01} and LP_{11} mode groups are well separated in the beginning of the taper, they however come closer at one point of the taper as seen in the inlet in fig 4. The difference in n_{eff} between mode 2 and mode 3 at this point is 1.78×10^{-4} and this happens at a taper width of 60 µm for this set of SM2000 and OFS CL fibers. Mode mixing could happen at this point, resulting in crosstalk between the

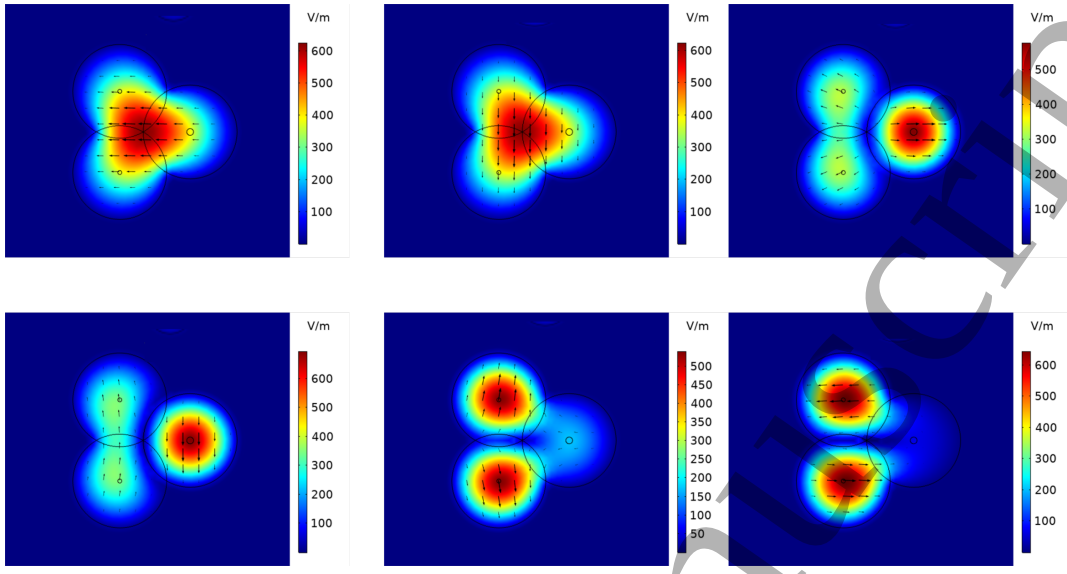

Figure 5. The mode distributions of the first six taper modes at a taper width of 19 µm.

two spatial channels. While designing PLs, fibers that give the largest n_{eff} difference at this closest point should be selected.

SM2000 fiber has a large core diameter of 11 µm and therefore the LP_{11} mode is slightly guided in the fiber. That is the reason why the n_{eff} values of mode 7 (magenta line in fig 5) is above the silica cladding (nclad) at the beginning of the taper, but the n_{eff} value is very close to the silica cladding index, so the mode will disappear after a few meters.

4.1. Overlap between taper modes and FMF modes

There should be maximum coupling of power between the taper modes and the FMF modes for the lanterns to work efficiently. The FMF is circular, but the taper end has a triangular shaped core. Due to the large index contrast between the air cladding and the silica core, the taper modes will be well confined within the silica core. The taper width that gives the highest overlap between the taper modes and FMF need to be found. The overlap between two normalized modes ψ_T and ψ_F are given as

$$O = \left| \iint_s \psi_T(x,y) \cdot \psi_F^*(x,y)\, dxdy \right|^2 \tag{2}$$

where it is assumed that the z component of the taper mode ψ_T and the FMF mode ψ_F are very small compared to the x and y components. Substituting the x and y components of the respective modes as:

$$\psi_T = \psi_{Tx}\hat{x} + \psi_{Ty}\hat{y} \tag{3}$$

$$\psi_F = \psi_{Fx}\hat{x} + \psi_{Fy}\hat{y} \tag{4}$$

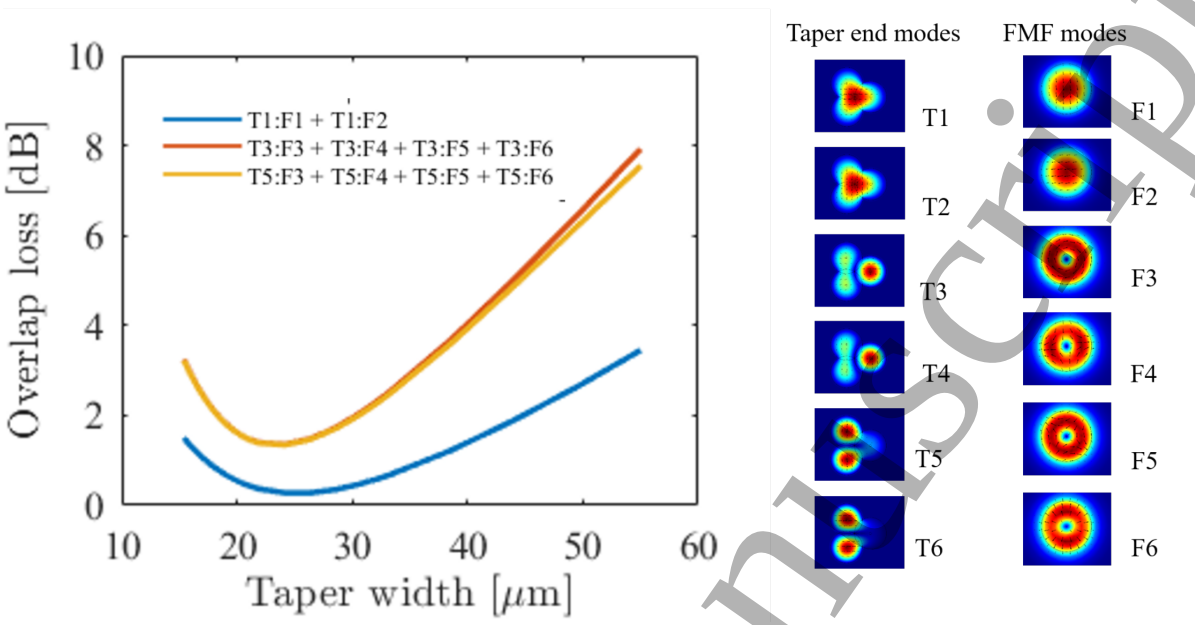

Figure 6. The variation of overlap loss for the taper modes and the modes of a FMF.

and including the normalization factors gives:

$$O = \frac{\left| \iint_s \left(\psi_{Tx}\psi^*_{Fx} + \psi_{Ty}\psi^*_{Fy} \right) \, dxdy \right|^2}{\iint_s \left(\psi_{Tx}\psi^*_{Tx} + \psi_{Ty}\psi^*_{Ty} \right) \, dxdy \iint_s \left(\psi_{Fx}\psi^*_{Fx} + \psi_{Fy}\psi^*_{Fy} \right) \, dxdy} \tag{5}$$

The x and y components of the mode distributions are extracted from the mode solver and the overlap integrals are calculated at different taper widths according to eqn 5. The results are shown in fig 6. The mode field distributions of the taper modes and FMF used for the overlap calculations are shown in the right side of fig 6. The overlap loss is minimum at a taper width of 24 μm. While fabricating the taper in the glass processor, the final taper width is set close to 24 μm, so that there will maximum power coupling between the taper modes and the FMF modes. The above calculations are repeated with the scalar mode solver, where the overlap integrals between the LP like taper modes and LP modes are calculated. The obtained results agree with the full vectorial calculation in COMSOL. This shows that the large index contrast between silica and air will not result in much error in the scalar approximation used in the scalar mode solver. The scalar LP modes can be calculated as linear combinations of vector modes using the basis shown in table 2.

LP modes	vector modes
LP_{01}	HE_{1l}
LP_{1l}^{odd} LP_{1l}^{even}	HE_{2l}^{odd} HE_{2l}^{even} TE_{0l} TM_{0l}
For $m > 1$ LP_{ml}^{odd} LP_{ml}^{even}	HE_{m+1l}^{odd} HE_{m+1}^{even} EH_{m-1l}^{odd} EH_{m-1l}^{even}

Table 2. LP modes and the corresponding vector modes.

4.2. Adiabatic criteria for taper transition

For lossless transformation of power from the SMF modes to the FMF modes, the taper transition should be gradual, obeying the adiabatic condition: [16, 17]

$$\left| \frac{2\pi}{\beta_1 - \beta_2} \frac{d\rho}{dz} \int_A \psi_1(x,y,z) \frac{\partial \psi_2(x,y,z)}{\partial \rho} \; dA \right| << \; 1 \tag{6}$$

where ψ_1 and ψ_2 are the normalized fields distributions of the two neighbouring modes, β_1 and β_2 are their respective propagation constants, $\rho(z)$ is the local taper diameter, z is the axial direction of propagation, and A is the fiber cross section. As the difference in propagation constant between the modes gets smaller, $\frac{d\rho}{dz}$ should be smaller to satisfy the adiabatic condition. The coupling between neighbouring modes can result in crosstalk between the modes. As seen in eqn 6, to reduce this coupling between the modes, the difference between the propagation constants of the two modes should be as large as possible and the overlap between the mode distribution of one mode and the longitudinal change in mode distribution of the other mode should be as small as possible. The required taper length increases with the number of modes in the taper. In the regions of the taper where the n_{eff} values of the neighbouring modes come closer, light in one mode can couple into the other mode. As seen in fig 5, this happens where the taper width is between 100 µm and 50 µm, where the modes expand beyond their individual cores. The adiabatic factor can grow beyond unity at this point. The adiabatic factor $\eta(z)$ is calculated for the mode selective taper with one SM2000 fiber and two OFS CL fibers using equation:

$$\eta(z) = \left| \frac{2\pi}{\beta_1 - \beta_2} \frac{d\rho}{dz} \int_A \psi_1(x,y,z) \frac{\partial \psi_2(x,y,z)}{\partial \rho} \; dA \right| \tag{7}$$

The calculated adiabatic factor η at different taper widths is shown in fig 7. At the beginning of the taper, the modes are well confined within the individual SMF cores and hence the adiabatic factor is low. As the taper width decreases, the modes start expanding out of the SMF cores, and the n_{eff} values of the modes come closer and hence

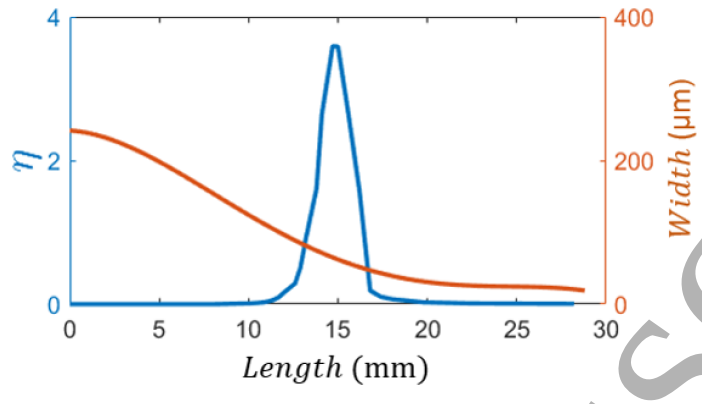

Figure 7. Variation of adiabatic factor as a function of taper length, for a three fiber taper with one SM2000 fiber and two OFS CL fibers.

Name	Core diameter [μm]	core index @1550
SSMF	9	1.4492
HI1060	5.3	1.4511

Table 3. The core diameter and refractive indices of SSMF and HI1060 fibers.

η increases as high as 3.6 at a taper width of 71 μm. The calculation is also repeated for another set of three fibers, namely one SSMF and two HI1060 fibers, with the core diameter and refractive index as shown in Table 3. The adiabatic behaviour for this set of fibers is similar, but η goes as high as 6 at a taper width of 100 μm. This shows that there will be larger mode coupling in this taper with one SSMF and two HI1060 fiber than in the taper with one SM2000 fiber and two OFS CL fibers. Measurements on the fabricated PLs also confirms this calculation.

5. Fabrication

The SMFs are tapered using a Vytran filament fusion splicer. The waist part of the taper is cleaved and spliced to a two mode step index (TMSI) fiber. A schematic of the fabrication is shown in fig 8. An FTAT3 graphite filament is used for tapering. Before tapering, the fibers are heated axially, so they are melt together [18]. The axial heating is made using the 'fire polish' routine of the splicer. After the axial heating, the melted fiber bundle is tapered, where the taper dimensions are set so that the final taper width is close to 24 μm. An image of a fabricated taper is shown in fig 9a. The tapered fiber bundle is cleaved at the waist part using a ruby hand cleaver. The cleaved taper end is shown in fig 9b. White light is launched to each of the SMFs of the taper and the taper end images are captured using the camera in the glass processor. The taper end images shown in fig 9c resemble the calculated mode distributions shown in fig 5. The cleaved tapered end is spliced to a 3.5 m TMSI fiber. This is a very dissimilar splice between

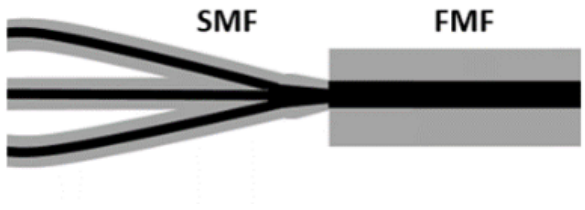

Figure 8. A schematic of the fabrication of a three fiber PL.

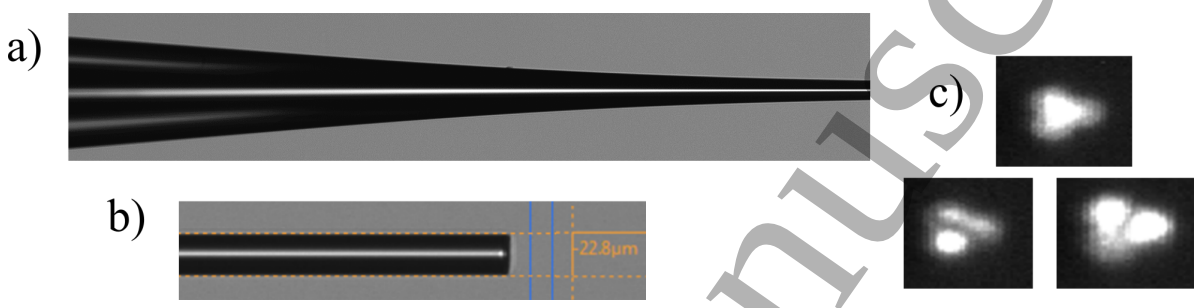

Figure 9. a) The fabricated three fiber taper b) Cleaved end of the taper c) The captured field images at the taper end, when white light is launched into each of the three SMFs.

the 23 μm tapered end and 125 μm TMSI fiber and is done using the FTAV2 filament in the Vytran glass processor. The splice parameters used for this dissimilar splice is shown in fig 10a . The splice power is smaller than that used for a normal SMF-SMF splice. The parameter called splice offset is set to 240 μm, so that that V2 filament is shifted 280 μm towards the 125 μm fiber. This is to avoid the thin 20 μm fiber end from getting heated up too much and burn back quicker than the 125 μm fiber. An image of the dissimilar splice is also shown in fig 10b. The spliced PL is taped to a plastic base with a groove in the middle to maintain the air cladding around the tapered part. A protective covering on the top is used to protect the tapered part from gathering dust. Although, the fabricated lantern is very fragile due to the dissimilar splice, after the PL is taped to the base, it will stay stable. A fabricated PL placed on the plastic base is shown in fig 11. This will help to avoid small bends on the taper that could vary the crosstalk of the device. Small vibrations and temperature changes in the laboratory do not affect the crosstalk much and this is confirmed by repeated measurements on the fabricated devices.

6. Characterization

6.1. Multiplexing crosstalk using S^2 imaging technique

Spectral and spatial (S^2) imaging technique is used for measuring the multiplexing crosstalk of the lantern. There are two LP mode groups in the TMSI fiber. Generally, crosstalk is defined as the ratio of power in the parasitic mode to the total power in both modes. Here, using the S^2 setup the relative power of the parasitic mode to the

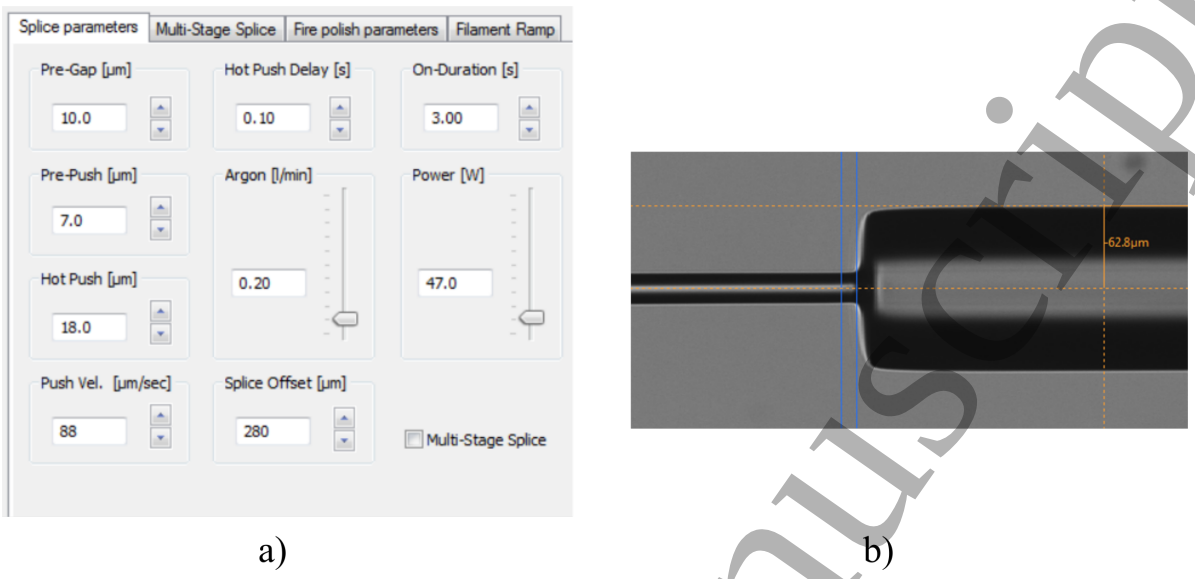

Figure 10. a) The splice parameters used for the dissimilar splice. b) The dissimilar splice between the 23 µm tapered end and 125 µm TMSI fiber.

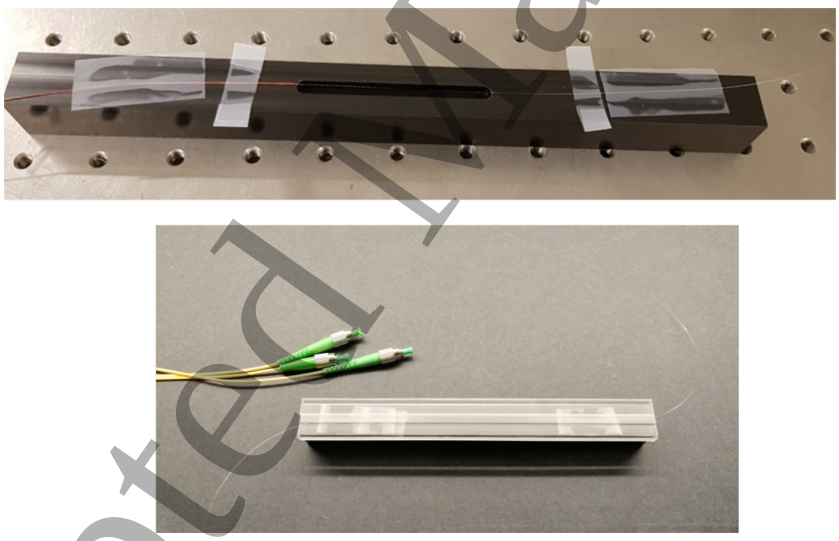

Figure 11. The fabricated PL with three SMFs.

dominant mode is calculated. As long as the dominant mode power is much higher than the parasitic mode power, the crosstalk can be approximated to the relative power of parasitic mode. The modes propagating in an optical fiber can be identified by the group delay difference (DGD) between the modes. When a broad band light is propagating through the fiber, this will result in a spectral interference pattern. There will also be a spatial interference pattern between the higher order modes and the fundamental mode in the fiber. This spectral and spatial interference allows the simultaneous imaging of multiple modes propagating in the fibers and to quantify their relative powers [19]. The S^2 data could be acquired using a tunable laser source and a CCD camera to capture the near field distribution out of the TMSI fiber [20]. If E_1 and E_2 are the electric field

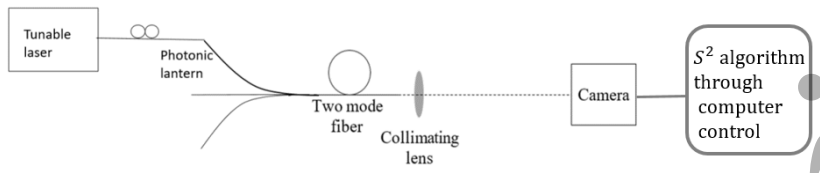

Figure 12. The set up used for S^2 measurement.

distributions of the two modes propagating in the TMSI fiber, which can be written as

$$E_1 = A_1(x, y) \exp -i\left(\beta_1 z + \phi_1(x, y)\right) \tag{8}$$

$$E_2 = A_2(x, y) \exp -i\left(\beta_2 z + \phi_2(x, y)\right) \tag{9}$$

where A_i is the transverse field distribution, β_i is the propagation constant and ϕ_i is the phase distribution of each modes with $i = 1, 2$. When the two modes are added together, $E = E_1 + E_2$, the total intensity $I = E \cdot E^*$ can be written as:

$$I(x, y, z) = I_1(x, y) + I_2(x, y) + 2A_1A_2 \cos(\Delta\beta z + \Delta\phi(x, y)) \tag{10}$$

Where I_1 and I_2 are the intensity of the individual modes and $\Delta\beta = \beta_1 - \beta_2$, and $\Delta\phi = \phi_1 - \phi_2$. Eqn 10 shows that the intensity pattern oscillates corresponding to $\Delta\beta$ of the two modes. $\Delta\beta z$ can be expanded using Taylor series as

$$\Delta\beta z \approx \Delta\beta_0 z - DGD\frac{2\pi c}{\lambda^2}\Delta\lambda \tag{11}$$

where the second and higher order derivatives are omitted. DGD is the differential mode delay between the two modes after the modes have propagated a distance z in the fiber. Thus, it could be seen that the intensity fluctuates with wavelength with a period [20].

$$\Delta\lambda = \frac{\lambda^2}{DGD \cdot c} \tag{12}$$

where λ is the central wavelength of light. The schematic of the measurement set up is shown in fig 12. The minimum DGD that can be measured using the setup depends on the bandwidth of the tunable laser. The maximum DGD that can be measured depends on the resolution of the spectral measurement. For this measurement, the Agilent 81689 tunable laser is tuned over 10 nm and the wavelength step used is 0.2 nm. When light is launched to SM2000 fiber, the dominant mode distribution at the end of TMSI fiber is LP_{01}. The reconstructed mode distributions of the dominant mode and parasitic mode are shown in fig 13. The fringes seen in the parasitic mode could be due to the reflections on the camera. When light is launched to either of the OFS CL fibers, a linear combination of LP_{11a} and LP_{11b} modes is the dominant field distribution. The corresponding reconstructed mode distributions are shown in fig 14. Here, the parasitic mode is LP_{01}, but the mode profile in fig 14b, does not look like an LP_{01} mode. The

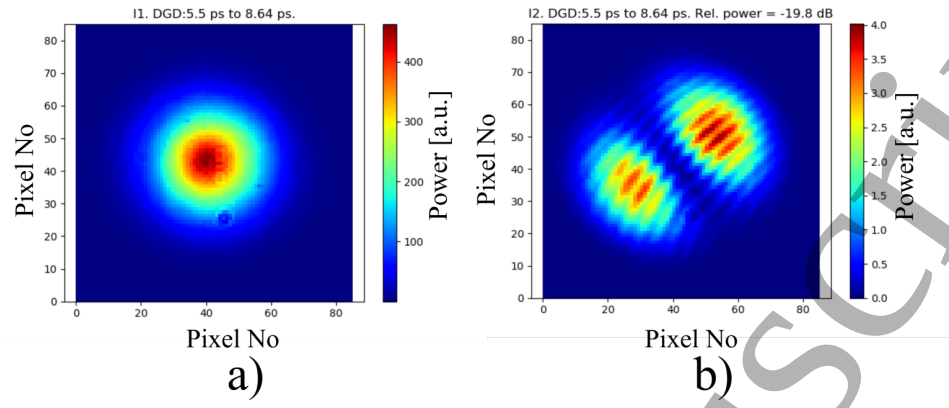

Figure 13. The regenerated mode distribution of the a) dominant mode and the parasitic mode in the TMSI fiber, when light is launched to the SM2000 fiber of the PL.

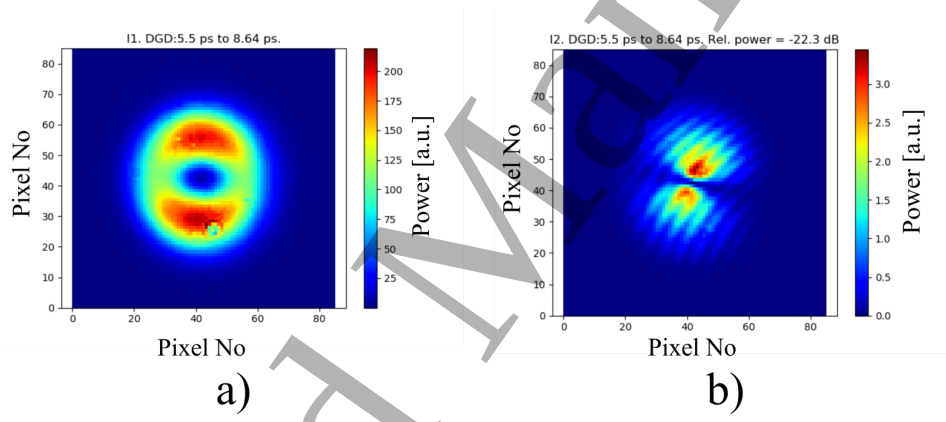

Figure 14. The regenerated mode distribution of the a) dominant mode and the parasitic mode in the TMSI fiber, when light is launched to one of the OFS CL fiber of the PL.

reason is that, S^2 algorithm calculates the amount of power in the parasitic mode from the amplitude of beating between the dominant mode and the parasitic mode. For this case LP_{11} is the dominant mode, which has no power in the middle, so it does not show any power in the middle of the reconstructed parasitic mode profile.

The polarization dependence of the device is characterized by changing the input polarization of light using an Agilent 11896A motorized polarization controller connected after the tunable laser in fig 12. The input polarization is randomly changed around 10 times and each time the dominant mode field distribution and relative power of the parasitic mode in the TMSI fiber is calculated. To check the broad band nature of the device, the wavelength range is varied from 1525 nm to 1575 nm. The measured crosstalk values for two PLs are shown in fig 15 [21, 22]. The results shown in fig 15a is for a PL fabricated with one SM2000 fiber and two OFS CL fibers and the results in fig 15b is for a PL fabricated with SSMF and HI1060 fibers. The crosstalk is lower for the SM2000 OFS CL combination of fibers. The adiabatic factor calculation given in

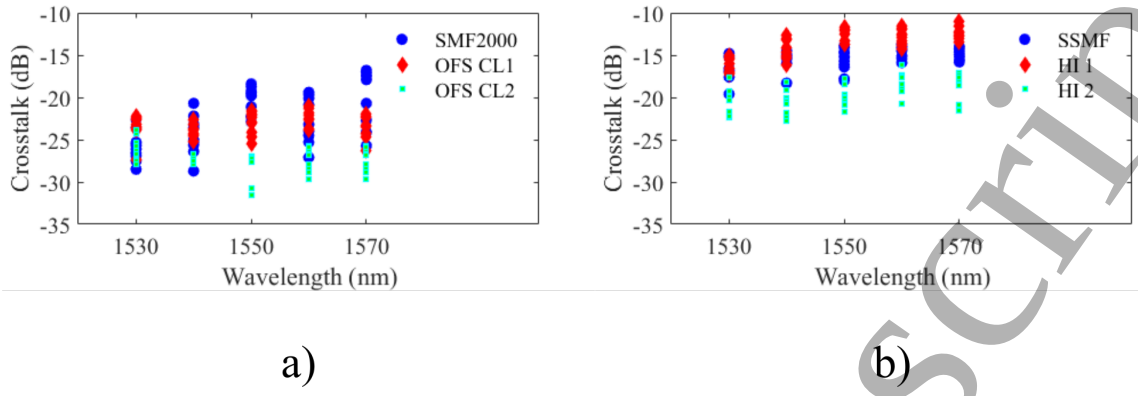

Figure 15. The multiplexing crosstalk measured using S^2 technique on PL fabricated with a) SM2000 and OFS CL fibers b) SSMF and HI1060 fibers.

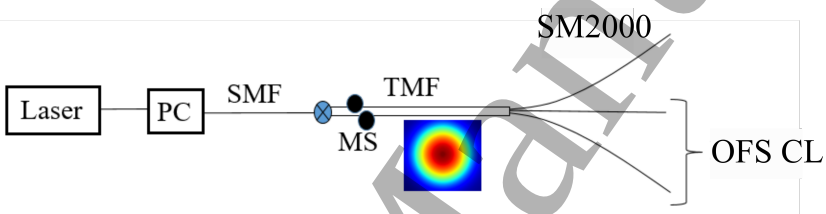

Figure 16. The setup used to launch LP_{01} mode into the TMSI for measuring the de-multiplexing loss of the PL for LP_{01} mode.

section 4.2 also showed larger mode coupling for the SSMF HI1060 fiber combination. In the fig 15, the three SMF input cases are shown in three different colors and for each inputs, the 10 random input polarization cases are shown in markers. The results show that the fabricated lanterns are polarization dependent. One reason for this variation of crosstalk with input polarization could be because the three fiber taper end is not circular, but triangular. The large index contrast between the air and silica will further confine the modes. A change in input polarization of light could change the overlap between the taper modes and the TMSI fiber modes. The slight misalignment in the splice could also introduce more polarization dependence.

6.2. De-multiplexing loss measurements

The de-multiplexing loss of the fabricated lanterns are measured by coupling light in a specific mode into the TMSI and measuring the power at the SM fibers. LP_{01} mode is launched into the TMSI fiber first, by splicing the TMSI fiber to an SM fiber. The TMSI is also bend around a mode stripper with two perpendicular bends of diameter less than 8 mm to remove any higher order mode that could still present in the TMSI fiber. The experimental setup is shown in fig 16. When LP_{01} mode is launched in the TMSI fiber, most of the LP_{01} power will be delivered to the large core, SM2000 fiber, and less power in the other two OFS CL fibers. The polarization dependent de-multiplexing loss is measured using a polarization scanning method [23]. The polarization controller is

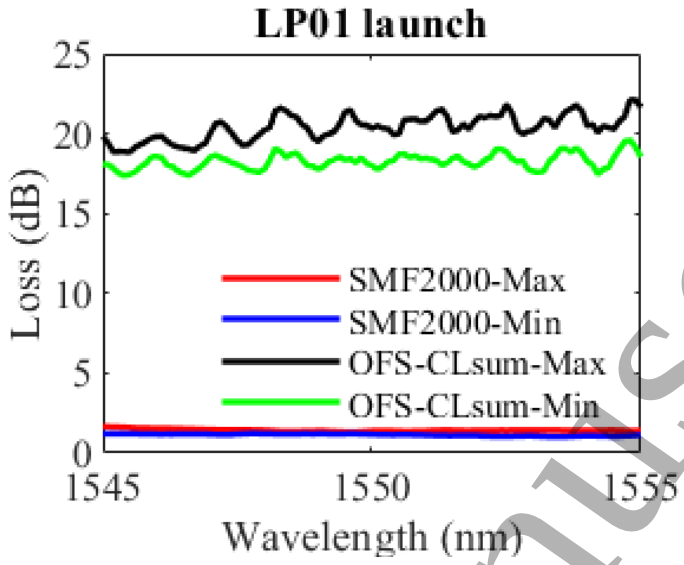

Figure 17. The PDL measurement on the PL in the demultiplexing direction, when LP_{01} mode is launched in the TMSI fiber

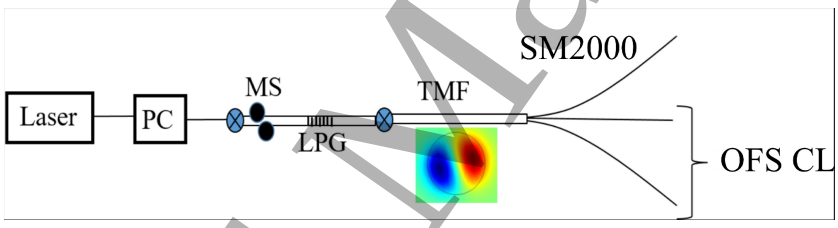

Figure 18. The setup used to launch LP_{11} mode in the TMSI, to measure the de-multiplexing loss for LP_{11} mode in the PL.

randomly changed for a time period of 10 s to make sure that all possible polarization states are covered and the output power is monitored. The maximum and minimum transmitted power is noted from the monitored values. The wavelength dependent polarization dependent de-multiplexing loss measured on the PL for LP_{01} mode is shown in fig 17. There is lower loss for the SM2000 fibers than the OFS CL fibers, showing the de-multiplexing capability of the PL for LP_{01} mode. The difference between the two losses is a measure of the relative power of the parasitic LP_{11} mode in the fiber.

LP_{11} mode is launched to the TMSI fiber next, using a long period grating (LPG) as shown in the set up in fig 18. A thermal induced LPG, where the LP_{01} mode is suppressed more than 15 dB, at wavelengths close to 1550 nm is used here [8, 24]. The PDL for the three SMFs are measured as before. When LP_{11} is launched in the TMSI fiber, there will be more power at the two OFS CL fibers and hence a lower loss. The measured wavelength dependent PDL for LP_{11} launch is shown in fig 19. The sum of powers at the two OFS Cl fibers is taken here, as either of the OFS CL fiber delivers a linear combination of LP_{11a} and LP_{11b} mode powers. When LP_{11} mode is launched to the TMSI fiber, there is lower loss for the OFS CL fibers than the SM2000 fibers, showing the

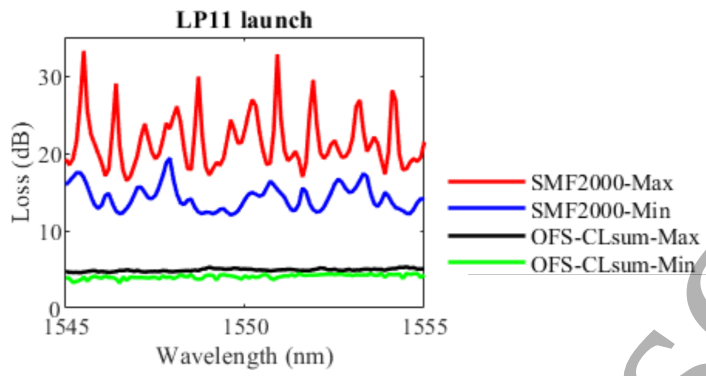

Figure 19. The PDL measurement on the PL in the demultiplexing direction, when LP_{11} mode is launched in the TMSI fiber

de-multiplexing capability of the lantern for the LP_{11} mode. However, the polarization dependency of the de-multiplexing loss is higher in this case. A change in polarization results in the rotation of LP_{11} mode [20]. This rotation will change the overlap of taper modes with FMF modes, resulting in larger variation in loss. The difference between the blue and black line in fig 19 gives the worst de-multiplexing crosstalk for LP_{11} mode as -9.4 dB. This is higher than the crosstalk for LP_{01} mode shown before in fig 17, which is -16.8 dB. These values are also higher than the crosstalk measured in the multiplexing direction using S^2 technique shown in fig 15a. This shows that the device behaves slightly differently in the multiplexing and de-multiplexing direction.
The multiplexing PDL (insertion loss) of the device is also measured from all the three SMF ends to the TMSI fiber over 1545 nm to 1555 nm. The average PDL for the SM2000 and the two OFS CL fibers are 0.66 dB - 0.95 dB, 2.9 dB - 3.2 dB and 4 dB - 4.3 dB respectively. Out of the two OFS CL inputs of the multiplexing PL, the one that give the lowest loss and lowest crosstalk can be used to launch the LP_{11} mode. On the other hand, while collecting the total LP_{11} power, both OFS CL ports of the de-multiplexing PL need to be used.

7. MDM transmission using air-clad PLs.

MIMO-less MDM transmission with two spatial channels is performed at different data rates using two fabricated PLs. Short reach applications like data center networks and interconnections for high speed computers are interested in this kind of MDM without MIMO [25]. Conventional intensity modulation and direct detection (IM-DD) are preferred in these short reach applications as they are simpler and cost efficient. Such kind of simple IM-DD transmission is tried with the air-clad PLs here. The MDM transmission setup is shown in fig 20. Light from a distributed feedback laser (DFB) is intensity modulated using a Mach Zehnder modulator (MZM). The amplified signal is split into two for the two spatial channels using a 3 dB coupler. A pattern generated generates pseudo random bit sequence of length $2^{31} - 1$. The DFB laser has a line

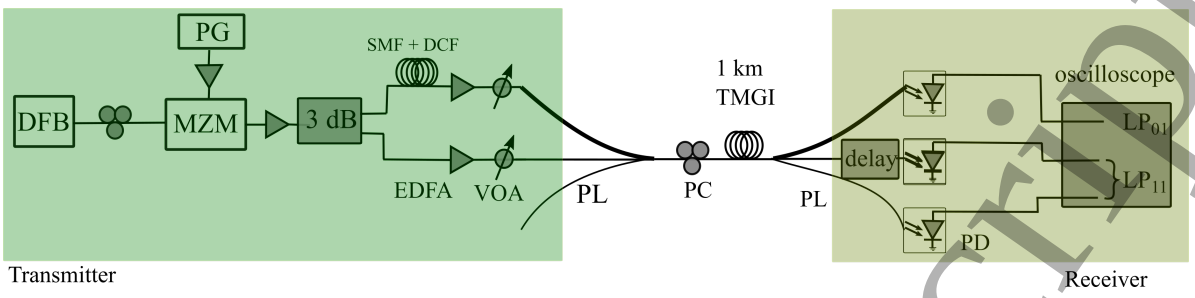

Figure 20. The setup used for MDM transmission of two spatial channels. DFB: Distributed feed back laser, PG: Pattern generator, MZM: Mach Zehnder modulator, EDFA: Erbium doped fiber amplifier, DCF: Dispersion compensation fiber, VOA: Variable optical attenuator, PL: Photonic lantern, PC: Polarization controller, PD: Photodiode.

width of a few MHz, which gives a coherence length around 100 m. A 2 km SMF+300 m dispersion compensation fiber is included in one of the spatial paths to exceed the coherence length of the laser, so that to avoid the interference between the modes at the photodiode. PLs fabricated with SSMF and HI1060 fibers are used here. The two spatial paths are separately amplified and fed to the SSMF and HI1060 fibers of the multiplexing lantern. For the fabricated lanterns, the LP_{11} path has higher loss than the LP_{01} path, hence variable attenuators are connected to each paths to balance the power in the two modes, so that the output power is the same in both channels. As shown before in section 6, the fabricated lanterns show polarization dependent crosstalk, hence a polarization controller is set on the TMSI to rotate the LP_{11} mode to get the lowest de-multiplexing crosstalk. Three modulation rates, namely 10, 25 and 40 Gb/s are used for the transmission. The output powers in the channels are measured using three photodiodes connected to the SMFs of the de-multiplexing PL, and the real time traces are acquired using a 33 GHz oscilloscope. The sampling speed of the oscilloscope is 80 GS/s. The output powers from the two HI1060 fibers of the de-multiplexing lantern are electrically added in the oscilloscope to get the total power in the LP_{11} mode. A free space delay is connected to one of the LP_{11} paths, to align the two LP_{11} traces in the two HI1060 fibers, before they are added. The MDM transmission quality is checked by finding the Q value of the output traces, calculated from the intensity distributions and the standard deviations of the 1 and 0 bits [26]. If I_1 and I_2 are the average intensity value for the 1 and 0 bits and σ_1 and σ_0 are the corresponding variances, the Q factor for the two intensity distributions is:

$$Q = \frac{I_1 - I_0}{\sigma_1 - \sigma_0} \tag{13}$$

where it is assumed that the 1 and 0 distributions obey Gaussian statistics. The Bit error rate (BER) of the transmission can be estimated from the Q value as [26]:

$$BER = \frac{1}{2} erfc\left(\frac{Q}{\sqrt{(2)}}\right) \tag{14}$$

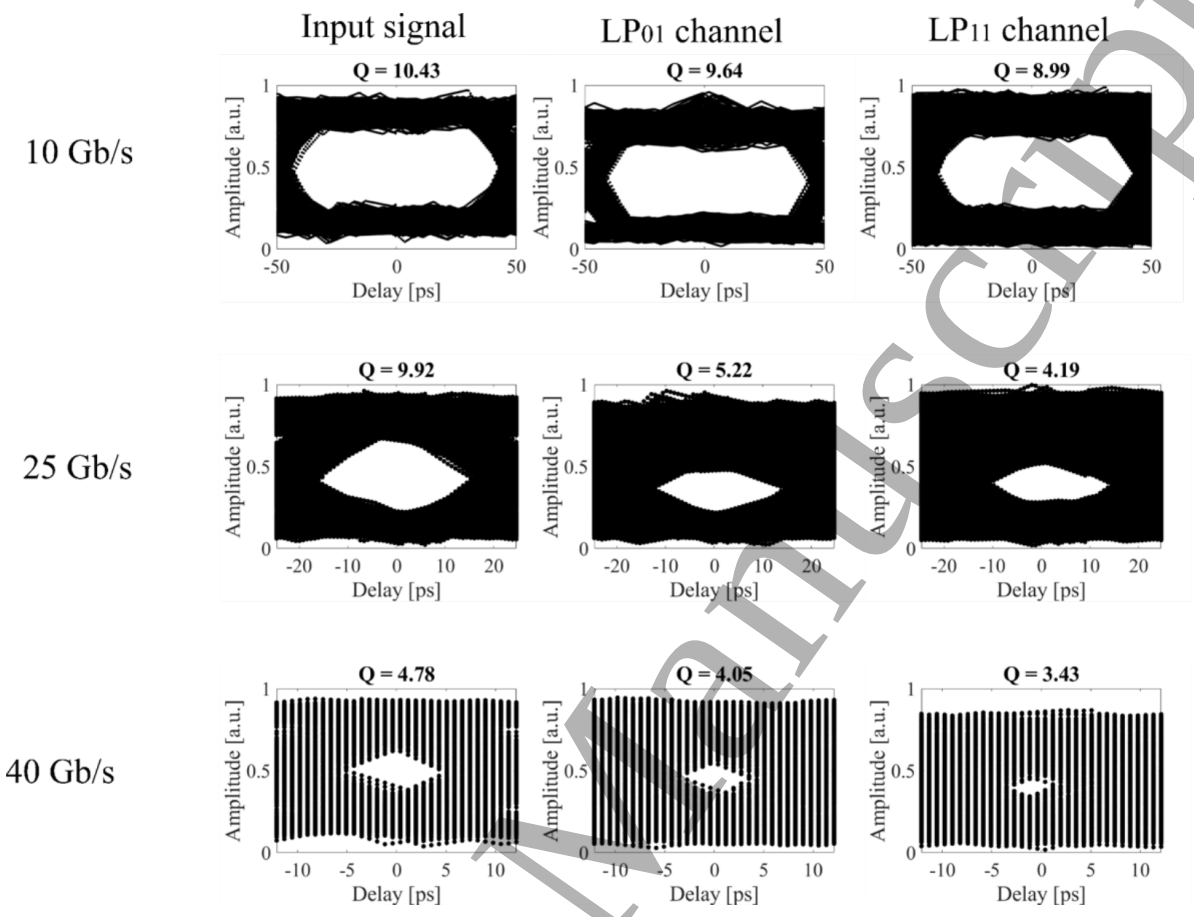

Figure 21. The obtained Q values and the eye diagrams for the input signal and the two output channels for transmissions at modulation rates of a) 10Gb/s b) 25 Gb/s and c) 40 Gb/s.

$erfc$ is the complementary error function

$$erfc(x) = \frac{2}{\sqrt{\pi}} \int_x^{\infty} -y^2 \, dy \tag{15}$$

The input traces fed to the multiplexing PL, is saved to compare it with the output traces and thereby assess the degradation. As the sampling speed of the oscilloscope is 80 GS/s, for higher modulation rates like 40 Gb/s, there will be only two samples per bit. Hence a linear interpolation with more points is made on the acquired signal values. The TMSI fiber end of two fabricated Pls are spliced together, which gives around 7 m of TMSI fiber between the two lanterns and data is transmitted simultaneously through the two spatial modes at different modulation rates. The obtained Q values and the eye diagrams for the two output channels and for the corresponding input signals fed to the multiplexing PL are shown in fig 21 [27]. A Q value of 6 corresponds to a BER of 10^{-9}, ie one bit out of a billion bits detected has gone wrong, which is considered as a good transmission performance. Results in fig 21 shows that for 10 Gb/s modulation rate, the calculated maximum Q for both LP_{01} and LP_{11} as good as that for the input signal. For 25 Gb/s, there is some degradation for the output signal. One reason for

this degradation could be that, the polarization controller at the TMSI fiber is not fully optimized to give the minimum de-multiplexing crosstalk. For 40 Gb/s modulation rate, the input signal to the multiplexing lantern, already has a low Q. This could be due to some instability in the transmitter. This band width of the oscilloscope is 33 GHz, which is close to the modulation rate. However, compared to the input signal, the output traces for 40 Gb/s modulation rate are not much degraded.

When the signal is modulated at 10 Gb/s, the band width of the oscilloscope used here is much larger than the wanted signal frequency. The unwanted frequencies present in the output signal can be removed by using a Gaussian filter on the received traces [28]. A nearly ideal 16th order super Gaussian filter is used to emulate the needed receiver bandwidth. The frequency response of the Gaussian filter is:

$$g(f) = \left(\exp - \frac{f^2}{2\sigma_f^2}\right)^n \tag{16}$$

n is the Gaussian order and

$$\sigma_f = \frac{\Delta f_{FWHM}}{2\sqrt[2n]{2^n \ln 2}} \tag{17}$$

Δf_{FWHM} is the FWHM bandwidth of the filter. The Q values for the output traces modulated at 10 Gb/s are calculated for different filter bandwidths. The highest Q value is obtained when the receiver bandwidth is same as the modulation rate. The result for the output trace of LP_{01} channel is shown in fig 22. The filter implementation on the Fourier transform of the LP_{01} output trace is shown in fig 22(b). These results also agree with the simulations on the influence of detector bandwidth on transmission performance reported in [28]. The effect of filtering on the two output traces are shown in fig 23. This is 10 Gb/s modulated signal and a Gaussian filter of bandwidth 9.5 GHz is used to remove the unwanted frequency components. The results show that, the implementation of the filter improves the Q of LP_{01} trace from 9.6 to 13.6 and for the LP_{11} trace, the Q is improved from 9 to 12.6.

As the next step, the FMF length between the PLs is increased by splicing a 1 km two mode graded index fiber (TMGI) between them. The data is modulated at 10 Gb/s and a filter bandwidth of 10 GHz is emulated at the receiver. The obtained Q and the eye diagrams for the input signal and the two output signals corresponding to the LP_{01} and LP_{11} channels for 1 km transmission through TMGI fiber are shown in fig 24. The obtained Q for the two channels are 5.39 ($\mathrm{BER}_Q = 3.5 \times 10^{-8}$) and 4.69 ($\mathrm{BER}_Q = 1.3 \times 10^{-6}$) respectively. Compared to the input signal, the output channels have lower Q. The results show that there is more degradation for 1 km transmission than for the 7 m transmission at the same modulation rate of 10 Gb/s shown before in fig 21a. As the fiber gets longer, the rotation of LP_{11} at the end of the fiber becomes faster. Hence, it is difficult to tune the polarization controller placed at the TMSI fiber fast enough to get the minimum de-multiplexing crosstalk at the second PL. This results in signal distortion. The mode coupling in the two splices between the TMSI and TMGI fibers is also another source for signal degradation.

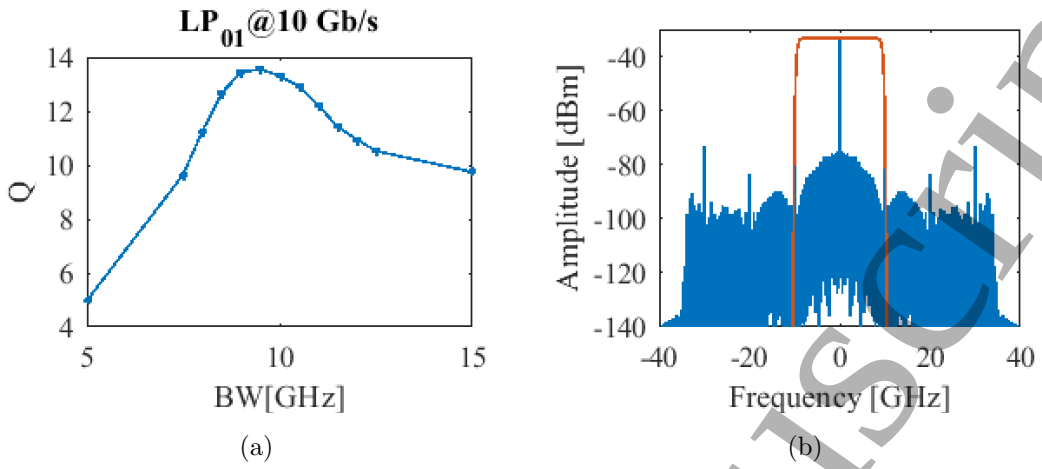

Figure 22. Low pass filtering of the output signal modulated at 10 Gb/s. a) The calculated Q values for the LP_{01} channel for different filter bandwidths. The best Q value is obtained at a filter bandwidth of 9.5 GHz b) The Fourier transform of the LP_{01} output signal shown in blue lines and the Gaussian filter of BW 9.5 GHz is shown in red line.

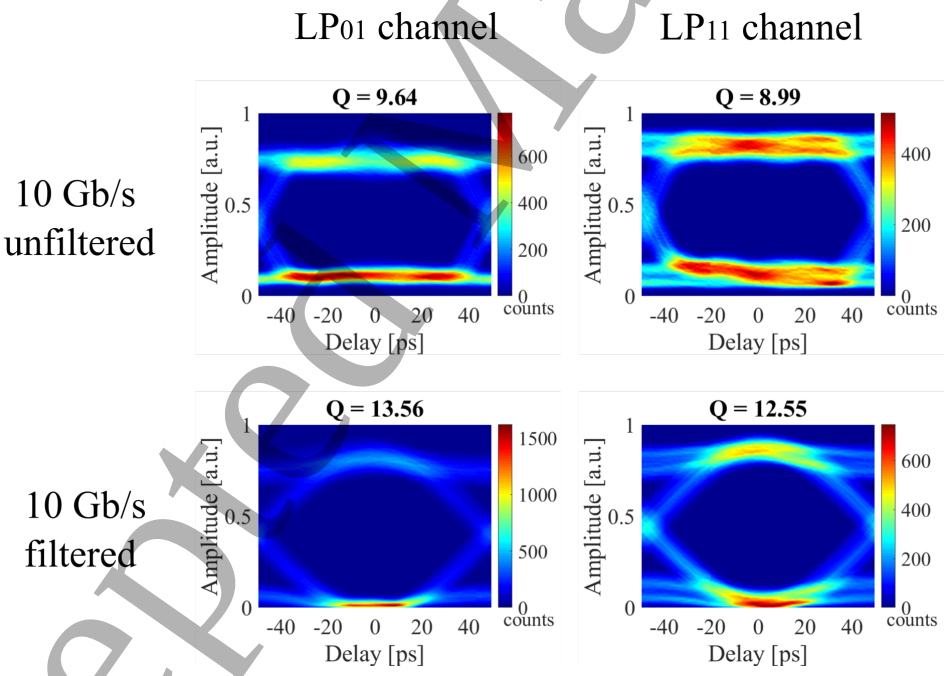

Figure 23. The Q values and the eye diagrams for the LP_{01} and LP_{11} output traces modulated at 10 Gb/s. A filter bandwidth of 9.5 GHz is used to emulate the optimum receiver bandwidth. Pcolor plots are used for the eye diagrams here, to show the density of signal value points.

7.1. MDM transmission using two lasers.

There are two sources for signal degradation in a MIMO-less MDM transmission. One is the crosstalk, where the field in one spatial mode adds itself to the field in the other mode, and the other source is the interference due to the modes beating with each

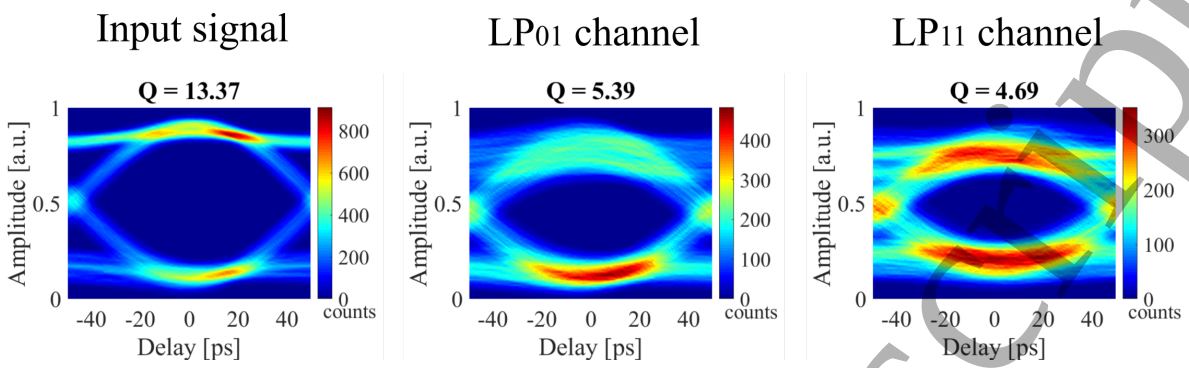

Figure 24. The calculated Q and the eye diagrams for the input signal, LP_{01} and LP_{11} for 1 km transmission through a TMGI fiber. The data is modulated at 10 Gb/s.

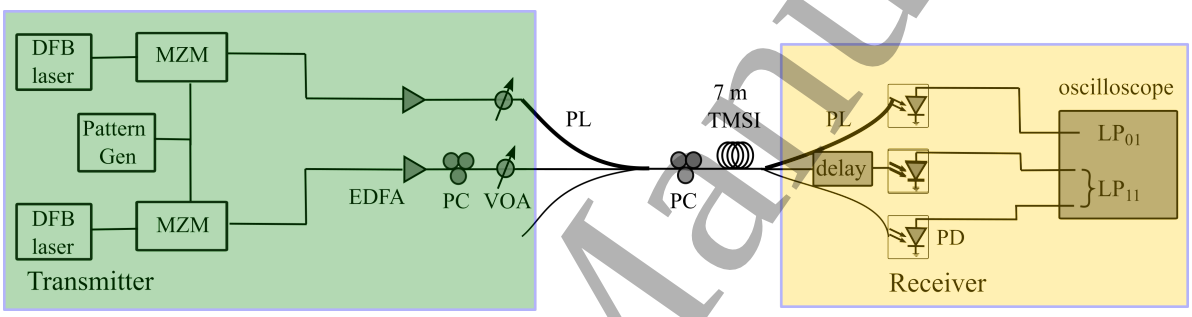

Figure 25. The MDM transmission setup using two lasers.

other [29]. In the transmission set up shown in fig 20, this modal noise is reduced by using a delay in one of the spatial paths by connecting a fiber with a length that could exceed the coherence length of the source. Another way to mitigate the modal interference is by using different wavelengths for the two modes, so that the wavelength spacing is large enough that the modal beat frequency becomes much larger than the detector bandwidth. This kind of wavelength interleaved FMF transmissions has already been reported [30, 31]. For 10 Gb/s modulation rate, a wavelength spacing of 0.2 nm is enough to mitigate the modal interference [28]. This is smaller than the grid spacing used in dense WDM systems, which is 50 GHz. Hence, wavelength interleaved MDM could be combined with WDM systems. An MDM transmission setup with two DFB laser sources, used to study these modal interference effects is shown in fig 25. Two DFB lasers are separately modulated and used for the two channels. One laser is set at a fixed wavelength and the other laser is tuned to get a wavelength spacing of 0.2 nm and 1 nm. The Q values obtained for the two channels with the two wavelength spacings are shown in table 4. The MZ modulator used to modulate the laser for the LP_{11} path is not that good compared to the one used for the LP_{01} path. This will result in more degradation for the LP_{11} channel. Hence the Q values for the input signals to both channels are given in table 4. Results of transmission using a single laser is also given in the last row. For this single laser transmission, a 1.7 km SMF is connected in one of the spatial path to decorrelate the two paths. The modulation rate used is

Table 4. The obtained Q values for the input signals and the output traces for the two spatial channels for different wavelength spacings and for the transmission using a single laser with a decorrelation fiber in one of the paths.

λ spacing nm	Q values for			
	Input signals to		Output signals from	
	LP_{01} channel	LP_{11} channel	LP_{01} channel	LP_{11} channel
0.2	18.7	7.9	9.4	6.4
1	19.5	7.7	12.8	7.4
single laser	21	19.8	6.1	5.7

10 Gb/s and the receiver band width is set to the same value as 10 GHz, using the Gaussian filter. The results show that, using wavelength interleaving on the two spatial paths, can improve the transmission performance better than using a single laser and a decorrelation fiber in one path. For the single laser transmission, the Qs for both input channels are very high, but the obtained Qs for the output traces are only 6.1 and 5.7, while for the 0.2 nm laser spacing, the obtained Qs for the LP_{01} and LP_{11} output traces are as high as 9.4 and 6.4. Note that the input signal to LP_{11} path for 0.2 nm spacing is only 7.9.

From the above MDM transmissions, it could be seen that the fabricated air-clad PLs could be used for multiplexing and de-multiplexing the two LP mode groups. The output signal traces can be further improved by using the correct receiver bandwidth. The degradation caused by modal beating can be reduced by using separate lasers with some wavelength spacing between them. The above MDM transmission is performed using PLs fabricated using one SSMF and two HI1060 fibers. In section 6, it was shown that PLs fabricated with one SM2000 fiber and two OFS CL fibers gives lower multiplexing and de-multiplexing crosstalk and lower polarization dependence. These optimized PLs are also used for MIMO-less MDM transmission through 1.6 km standard 50/125 μm multimode fiber [32]. The obtained Qs for both output channels are higher than 3.7 ($BER_Q = 1.1 \times 10^{-4}$), for all input polarizations. There was no need to use a polarization controller on the multimode fiber to select the the best polarization in this case. The modulation rate used is 10 Gb/s and a laser spacing of 2.1 nm is used for this transmission.

8. Conclusion

The design and fabrication steps for a new kind of photonic lantern is presented in this tutorial. The fabricated PLs can multiplex and de-multiplex two LP mode groups in a multimode fiber. The polarization dependent crosstalk of the lantern is measured using

spatial and spectral imaging technique. A crosstalk below -16.8 dB is measured over all polarizations, over a wavelength from 1525 nm to 1575 nm. The insertion loss of the device measured for LP_{01} and LP_{11} modes are 0.95 dB and 3.19 dB respectively. The fabricated lanterns are tested on mode division multiplexing transmission set ups. 2× 10 Gb/s MIMO-less MDM transmission is performed through 1.6 km standard 50/125 µm multimode fiber. A Q value higher than 3.7 ($BER_Q = 1.1 \times 10^{-4}$) is obtained for all input polarizations. 2× 40 Gb/s transmission is also demonstrated through two mode step index fiber of length 7m.

9. References

[1] K. C. Kao and G. A. Hockham, "Dielectric-fibre surface waveguides for optical frequencies."

[2] V. W. S. Chan, "In memory of charles kao kuen," *J. Opt. Commun. Netw.*, vol. 10, pp. ED1–ED1, Nov 2018.

[3] Cisco Annual Report. `https://www.cisco.com/c/en/us/solutions/collateral/executive-perspectives/annual-internet-report/white-paper-c11-741490.html#Trends`.

[4] J. Laegsgaard, *Introduction to dielectric waveguides, Numerical Methods in Photonics, DTU Fotonik*. 2014.

[5] L. Gruner-Nielsen, Y. Sun, J. W. Nicholson, D. Jakobsen, K. G. Jespersen, R. Lingle, and B. Palsdottir, "Few mode transmission fiber with low dgd, low mode coupling, and low loss," *Journal of Lightwave Technology*, vol. 30, no. 23, pp. 3693–3698, 2012.

[6] C. Koebele, M. Salsi, D. Sperti, P. Tran, P. Brindel, H. Mardoyan, S. Bigo, A. Boutin, F. Verluise, P. Sillard, M. Astruc, L. Provost, F. Cerou, and G. Charlet, "Two mode transmission at 2x100gb/s, over 40km-long prototype few-mode fiber, using lcos-based programmable mode multiplexer and demultiplexer," *Opt. Express*, vol. 19, pp. 16593–16600, Aug 2011.

[7] N. Barré, B. Denolle, P. Jian, J.-F. Morizur, and G. Labroille, "Broadband, mode-selective 15-mode multiplexer based on multi-plane light conversion," in *Optical Fiber Communication Conference*, p. Th2A.7, Optical Society of America, 2017.

[8] L. Grüner-Nielsen, N. M. Mathew, and K. Rottwitt, "Direct measurement of polarization dependency of mode conversion in a long period grating," in *Optical Fiber Communication Conference (OFC) 2019*, p. Th2A.15, Optical Society of America, 2019.

[9] An Li, A. Al Amin, Xi Chen, and W. Shieh, "Reception of mode and polarization multiplexed 107-gb/s co-ofdm signal over a two-mode fiber," in *2011 Optical Fiber Communication Conference and Exposition and the National Fiber Optic Engineers Conference*, pp. 1–3, 2011.

[10] S. Jiang, C. Liang, L. Ma, J. Xiong, W. Zhang, and Z. He, "Ultra-low-loss broadband all-fiber mode selective couplers for mimo-less mdm transmission," *Journal of Lightwave Technology*, vol. 38, no. 8, pp. 2376–2382, 2020.

[11] D. Noordegraaf, P. M. W. Skovgaard, M. D. Maack, J. Bland-Hawthorn, R. Haynes, and J. Lægsgaard, "Multi-mode to single-mode conversion in a 61 port photonic lantern," *Opt. Express*, vol. 18, pp. 4673–4678, Mar 2010.

[12] R. Ryf, N. K. Fontaine, M. Montoliu, S. Randel, B. Ercan, H. Chen, S. Chandrasekhar, A. H. Gnauck, S. G. Leon-Saval, J. Bland-Hawthorn, J. R. Salazar-Gil, Y. Sun, and R. Lingle, "Photonic-lantern-based mode multiplexers for few-mode-fiber transmission," in *OFC 2014*, pp. 1–3, 2014.

[13] J. C. Alvarado-Zacarias, N. K. Fontaine, J. E. Antonio-Lopez, Z. S. Eznaveh, M. S. Habib, H. Chen, R. Ryf, D. Van Ras, P. Sillard, C. Gonnet, A. Amezcua-Correa, S. G. Leon-Saval, and R. A. Correa, "Mode selective photonic lantern with graded index core," in *2018 Optical Fiber Communications Conference and Exposition (OFC)*, pp. 1–3, 2018.

[14] N. M. Mathew, L. Grüner-Nielsen, M. A. U. Castaneda, and K. Rottwitt, "A novel fabrication method for photonic lanterns," in *Optical Fiber Communication Conference*, p. M4D.4, Optical Society of America, 2018.

[15] N. M. Mathew, L. Grüner-Nielsen, M. A. U. Castaneda, M. Galili, and K. Rottwitt, "Mode-group selective air-clad photonic lantern," in *Frontiers in Optics / Laser Science*, p. FTu5B.4, Optical Society of America, 2018.

[16] J. D. Love, W. M. Henry, W. J. Stewart, R. J. Black, S. Lacroix, and F. Gonthier, "Tapered single-mode fibres and devices. i. adiabaticity criteria," *IEE Proceedings J - Optoelectronics*, vol. 138, no. 5, pp. 343–354, 1991.

[17] S. Yerolatsitis, I. Gris-Sánchez, and T. A. Birks, "Adiabatically-tapered fiber mode multiplexers," *Opt. Express*, vol. 22, pp. 608–617, Jan 2014.

[18] U. patent no.005935288A, *Method for producing fused fiber bundles*. 1997.

[19] J. W. Nicholson, A. D. Yablon, S. Ramachandran, and S. Ghalmi, "Spatially and spectrally resolved imaging of modal content in large-mode-area fibers," *Opt. Express*, vol. 16, pp. 7233–7243, May 2008.

[20] L. Grüner-Nielsen, N. Mathew, and K. Rottwitt, "Invited paper: Characterization of few mode fibers and devices," *Optical Fiber Technology*, vol. 52, Nov. 2019.

[21] N. M. Mathew, L. Grüner-Nielsen, M. Galili, M. Lillieholm, M. A. U. Castaneda, and K. Rottwitt, "Polarization dependence of mode-group selective air-clad photonic lantern," in *Optical Fiber Communication Conference (OFC) 2019*, p. Th3D.6, Optical Society of America, 2019.

[22] N. M. Mathew, J. B. Christensen, L. Grüner-Nielsen, M. Galili, and K. Rottwitt, "Air-cladded mode-group selective photonic lanterns for mode-division multiplexing," *Opt. Express*, vol. 27, pp. 13329–13343, Apr 2019.

[23] Yihong Zhu, E. Simova, P. Berini, and C. P. Grover, "A comparison of wavelength dependent polarization dependent loss measurements in fiber gratings," *IEEE Transactions on Instrumentation and Measurement*, vol. 49, no. 6, pp. 1231–1239, 2000.

[24] P. Akrami, L. Grüner-Nielsen, L. S. Rishøj, and K. Rottwitt, "Fabrication of heat-induced long-period gratings for mode conversion in few-mode fibers," in *Next-Generation Optical Communication: Components, Sub-Systems, and Systems X* (G. Li and K. Nakajima, eds.), vol. 11713, pp. 13 – 20, International Society for Optics and Photonics, SPIE, 2021.

[25] W. Wang, J. Zhao, L. Zhang, Q. Mo, Z. Yang, C. Li, Z. Wang, Z. Zhang, C. Carboni, and G. Li, "4 × 10-gb/s mimo-free polarization and mode group multiplexing for data center applications," *IEEE Photonics Technology Letters*, vol. 29, no. 20, pp. 1711–1714, 2017.

[26] G. Agrawal, *Fiber-Optic Communication Systems: Fourth Edition*. 01 2012.

[27] N. M. Mathew, L. Grüner-Nielsen, M. Galili, M. Lillieholm, and K. Rottwitt, "Mdm transmission using air-clad photonic lanterns," *IEEE Photonics Technology Letters*, vol. 32, no. 17, pp. 1049–1052, 2020.

[28] L. Grüner-Nielsen, N. M. Mathew, M. Lillieholm, M. Galili, and K. Rottwitt, "Modeling of mimo less mode division multiplexed systems," *IEEE Photonics Technology Letters*, vol. 32, no. 18, pp. 1191–1194, 2020.

[29] N. M. Mathew, L. Grüner-Nielsen, M. Galili, M. Lillieholm, and K. Rottwitt, "Cross talk and interference in mimo less few mode transmission systems," in *Conference on Lasers and Electro-Optics*, p. JW2E.24, Optical Society of America, 2020.

[30] K. Benyahya, C. Simonneau, A. Ghazisaeidi, N. Barré, P. Jian, J.-F. Morizur, G. Labroille, P. Sillard, J. Renaudier, and G. Charlet, "5tb/s transmission over 2.2 km of multimode om2 fiber with direct detection thanks to wavelength and mode group multiplexing," in *Optical Fiber Communication Conference*, p. M2D.2, Optical Society of America, 2017.

[31] Z. Wu, J. Li, Y. Tian, D. Ge, J. Zhu, Y. Zhang, J. Yu, Z. Li, Z. Chen, and Y. He, "3×4×10-gb/s mdm-wdm transmission over 21-km om3 mmf with ook modulation and direct detection," in *Optical Fiber Communication Conference*, p. W4J.3, Optical Society of America, 2018.

[32] L. Grüner-Nielsen, N. M. Mathew, M. H. Nymann, M. Lillieholm, M. Galili, and K. Rottwitt,

"Mode division multiplexing on standard 50/125 µm multi mode fiber using photonic lanterns," in *Optical Fiber Communication Conference (OFC) 2021*, p. W6A.41, Optical Society of America, 2021.